

Effects of Suction Parameters on Junction Flow

Shakeel Ahmed ¹, Abdullah Malik ¹ and Khalid Parvez ¹

Abstract—Formation of horseshoe vortex in the wing-body junction region is the major contributing factor in aerodynamic losses. Controlling horseshoe vortex using different schemes including localized suction ahead of the wing is under investigation for quite some time using wind tunnels and CFD techniques. Studies have shown that RANS prediction of the junction flow demonstrate a satisfactory qualitative comparison with experimental results. Similarly, Reynolds-Averaged Navier-Stokes (RANS) based turbulence model Spalart Allmaras can capture the basic flow features with and without localized suction indicating a satisfactory qualitative comparison with reference experiment for all suction rates. Localized suction is applied through a suction hole and is a proven active technique in removal of junction horseshoe vortex. The present study extends the CFD analyses of junction flow with localized suction to investigate the effects of suction hole parameters on formation of horseshoe vortex in the junction region. In order to evaluate the effect of suction hole location and dimensions on horseshoe vortex formation, localized suction with varying suction velocities have been applied through suction holes with two different dimensions placed at two different distances from the model leading edge. It has been observed that location of suction hole has a strong influence on formation of horseshoe vortex. Positioning the suction hole closer to the wing leading edge proves to be more effective in elimination of horseshoe vortex as lower suction rates are required to eliminate the vortex core as compared to the suction hole positioned away from the leading edge. Moreover, bigger dimensions of suction hole proved to be more effective in controlling the horseshoe vortex as compared with the smaller dimensions of suction hole.

Index Terms—Flow control, Horseshoe vortex, Junction flow, Localized suction, Suction parameters

I. INTRODUCTION

The turbulent complex flow around the wing body intersection is known as junction flow. It occurs whenever a boundary layer growing on a flat plate like surface is encountered with an obstruction in the surface. This type of flow suffers from secondary flows such as horseshoe vortices and corner separations that can dramatically harm the performance of aircraft [1]. Horseshoe vortex changes the flow behavior and causes aerodynamic losses in the junction region [2]. It is an important feature of junction flows and is a highly investigated area. This type of vortex forms when two-dimensional flow separations transform into three-dimensional complex flows due to interaction between the approaching boundary layers and the pressure field produced by the wing.

This horseshoe vortex originates from a stagnation point ahead of the wing and wraps around the whole wing [3]. In order to improve the aerodynamic efficiency of the junction flow, controlling this unwanted vortex formation through various active and passive schemes is a subject of investigation for quite some time.

In one study, Philips et al. [3] employed localized suction ahead of the wing leading edge in the subsonic wind tunnel experiment to eliminate the boundary layer which essentially removes the spanwise vorticity. They succeeded to significantly minimize the size and strength of the horseshoe vortex using the active control scheme. Barberis et al. [4] employed suction holes at different locations on symmetric plane ahead of the wing leading edge and concluded that applying suction in this manner significantly reduces the horseshoe vortex strength. They performed the experiments in a subsonic wind tunnel. Paciorri et al. [5] numerically simulated the junction flow using Spalart Allmaras and k-epsilon turbulence models and established that CFD can predict the junction flow with sufficient qualitative accuracy and hence CFD may be utilized for understanding vortex formation in the wing-body junction flows. J. L. Coombs et al. [6] evaluated the performance of various turbulence models for a junction flow test case using incompressible RANS simulations and showed that RANS based turbulence models are able to give acceptable results in comparison to the experimental data. A. M. Levchenya et al. also numerically simulated the occurrence of horseshoe vortex in the junction region using original and modified versions of RANS based Menter SST model [7]. They found out that these models produce qualitatively correct results when compared with the wind tunnel measurements.

S. Ahmed et al. [8] extended the study of junction flow by including localized suction in the numerical simulation of junction flows and concluded that RANS based one equation turbulence model Spalart Allmaras can capture the basic flow features with and without localized suction. This indicated a satisfactory qualitative comparison with reference experiment for all suction rates investigated; however, the quantitative comparison is not as good. Further, in comparison to the experimental results the qualitative predictions of low suction rates are better as compared to higher suction rates.

A Aim and Approach

The present study is an extension of junction flow analyses

Manuscript received: 16th February 2021.

¹ Dept. of Aeronautics and Astronautics, Institute of Space Technology, Islamabad

* Corresponding Author e-mail: shakeel6787@gmail.com.

with localized suction performed by S. Ahmed et al. [8] in which the effects of suction hole parameters on junction flow horseshoe formation has been explored. In this regard, effect of suction hole location and its dimensions on horseshoe vortex formation have been investigated by performing RANS simulations using one equation Spalart Allmaras [9] turbulence model. Moreover, effect of the incoming velocity on junction flow has also been examined. Numerical simulations have been performed using the commercially available CFD software Fluent [10]. Results obtained from this study may be utilized in understanding the effects of suction parameters for enhancing aerodynamic efficiency of junction flows through elimination of the unwanted horseshoe vortex.

II. NUMERICAL METHODOLOGY

Navier Stokes equations are solved together with continuity equation as the governing equations of all fluid flows. These equations are subjected to the laws of conservation of mass, momentum, and energy. In Reynolds averaging, the exact Navier Stokes equations are divided into mean and fluctuating parts. However, doing so produces additional terms in the N-S equations to represent the effects of turbulence. The additional terms are solved by introducing turbulence modeling equations. Spalart Allmaras turbulence model is a one equation model which has been used in this study to perform the numerical simulations in ANSYS Fluent. Transport equation for Spalart Allmaras model is shown below in Eq. 1.

$$\frac{\partial}{\partial t}(\rho\tilde{v}) + \frac{\partial}{\partial x_i}(\rho\tilde{v}u_i) = G_v + \frac{1}{\sigma_{\tilde{v}}}\left[\frac{\partial}{\partial x_j}\left\{(\mu + \rho\tilde{v})\frac{\partial\tilde{v}}{\partial x_j}\right\} + C_{b2}\rho\left(\frac{\partial\tilde{v}}{\partial x_j}\right)^2\right] - Y_v + S_{\tilde{v}} \quad (1)$$

Where, G_v is the production of turbulent viscosity and Y_v is the destruction of turbulent viscosity that occurs in the near-wall region due to wall blocking and viscous damping. $\sigma_{\tilde{v}}$ and C_{b2} are constants and \tilde{v} is the molecular kinematic viscosity. $S_{\tilde{v}}$ is a user defined source term. More details about the turbulence model can be found in the used software user's guide [11].

III. MODEL DESCRIPTION, SUCTION CONFIGURATIONS AND BOUNDARY CONDITIONS

A. Model Description and Computational Domain

This is an extension of the work performed by S Ahmed et al. [8]; therefore, same model and computational domain is utilized in their work has been used in this study as well. The wing model is a cylindrical obstacle of 360 mm diameter at the leading edge ending in a shaped trailing edge. The model had a total chord length of 1090 mm and height of 940 mm [8]. Half wing geometry with the same dimensions modeled for numerical simulations is shown in Fig 1.

Computational domain consists of a rectangular box inside which the wing model is placed at a distance of 3000 mm from the inlet on the center line of the section to get a symmetric flow. Domain extends 6000 mm downstream of the wing trailing edge to avoid back flow at the outlet during numerical

simulation. Suction holes of different configurations i.e., varying sizes are positioned ahead of the wing leading edge on the center line to provide localized suction for controlling the horseshoe vortex. Three-dimensional view of the computational domain is shown in Fig 2. This is the same computational domain used in [8]; however, location and dimension of suction hole have been varied according to the suction configuration requirements in different cases.

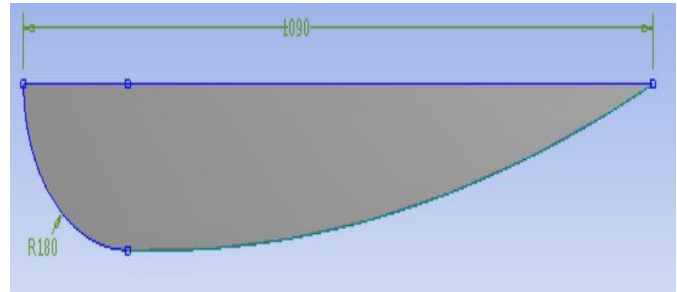


Fig 1 : Aerofoil of the Wing Model as appeared in [8].

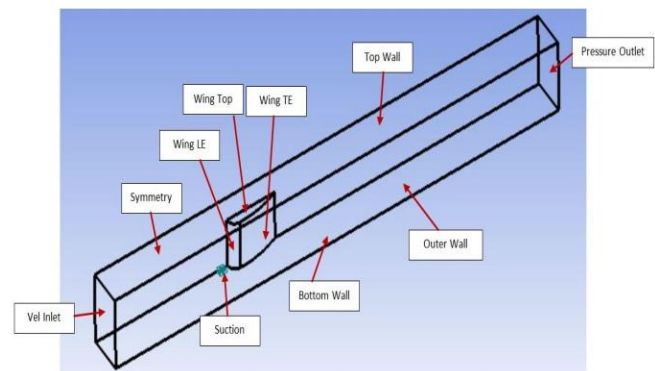


Fig 2 : Computational Domain as appeared in [8].

B. Suction Configurations

Two different dimensions of suction holes at two different locations have been numerically investigated during this research. For all the configurations, two different incoming velocities of 50 m/s and 25 m/s were simulated for each suction velocity case.

First configuration of suction hole with a dimension of $100 \times 82 \text{ mm}^2$ was located at 92 mm away from the wing leading edge, similar to the configuration used by Barberis et al. [4]. Six cases including the no suction and velocities of suction with a rate of five, ten, twenty, forty and fifty-five meters per second were simulated with 50 m/s incoming velocity for the first configuration by S. Ahmed et al. [8]. In this study all the six cases have been simulated again with 25 m/s incoming velocity.

In the second configuration, same suction hole with dimension $100 \times 82 \text{ mm}^2$ was moved closer to the wing at a distance of 50 mm from the wing leading edge. Five cases of suction velocities with a rate of five, ten, twenty, forty and fifty-five meters per second have been simulated with 50 m/s and 25 m/s incoming velocities for this configuration.

In the third configuration, suction hole dimension was reduced to almost half and changed to $50 \times 40 \text{ mm}^2$ and

positioned at a distance of 92 mm from the wing leading edge. Five cases of suction velocities with a rate of five, ten, twenty, forty and fifty-five meters per second have been simulated with 50 m/s and 25 m/s incoming velocities for this configuration as well.

In the fourth configuration, suction hole of the reduced dimension $50 \times 40 \text{ mm}^2$ was moved closer to the wing and positioned at a distance of 50 mm from the wing leading edge. For this last configuration five cases of suction velocities with a rate of five, ten, twenty, forty and fifty-five meters per second have been simulated with incoming velocity of 50 m/s. Suction configurations with incoming velocities and different suction velocities cases are summarized in TABLE I. It is pertinent to mention that suction velocities have been assigned negative sign in order to simulate outflow.

TABLE I
Summary of Numary of Numerically Simulated Cases

Configuration	Incoming Velocity	Suction Velocities (m/s)
First	50 m/s	0, -5, -10, -20, -40, -55
	25 m/s	0, -5, -10, -20, -40, -55
Second	50 m/s	-5, -10, -20, -40, -55
	25 m/s	-5, -10, -20, -40, -55
Third	50 m/s	-5, -10, -20, -40, -55
	25 m/s	-5, -10, -20, -40, -55
Fourth	50 m/s	-5, -10, -20, -40, -55

C. Boundary Conditions

The faces covering the computational domain were given names for identification as shown in Fig 2. Boundary conditions on all the faces (except “vel inlet” and “suction”) were same for all the cases. Summary of the boundary conditions are given in TABLE II. It is important to note that for no suction case the face was selected as no slip wall and for cases with suction, it was selected as velocity inlet and given the values with negative sign (to simulate outflow). Reynolds number for the flow was chosen as 3×10^6 based on the chord length of the wing geometry employed in this study and is kept similar to the Reynolds number used by Barberis et al. [4] in their study which was taken as a benchmark paper by S. Ahmed et al. [8].

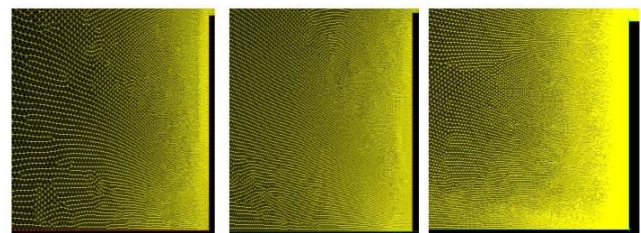
IV. GRID INDEPENDENCE

Grid independence study has been carried out at the wing incidence angle of 0° to the incoming velocity of 50 m/s. This investigation focused on the effects of grid changes on the three primary aerodynamic coefficients, i.e., lift, drag and pitching moment on the wing model surface. Moreover, capability of the grid to capture the formation of vortex core in front of the wing leading edge was also evaluated. Three grids named as coarse grid, fine grid, and superfine grid were generated for this purpose. Total number of cells for the coarse grid was 3.42

million, for fine grid was 4.83 million and for super fine grid was 5.98 million. Zoomed in view of the surface mesh of the symmetry plane near the wing leading edge for the three grids are shown in Fig 3.

TABLE II
Boundary Conditions

Face Name	Boundary Condition	Value	Remarks
Vel Inlet	Velocity Inlet	50 m/s, 25 m/s	Different Incoming Vel
Pressure outlet	Pressure Outlet	“0” gauge pressure	For all cases
Outer Wall	Wall	No Slip	For all cases
Bottom Wall	Wall	No Slip	For all cases
Top Wall	Wall	No Slip	For all cases
Wing LE	Wall	No Slip	For all cases
Wing TE	Wall	No Slip	For all cases
Wing Top	Wall	No Slip	For all cases
Symmetry	Symmetry	Symmetry	For all cases
Suction	Wall	No Slip	For no suction
	Velocity Inlet (<i>z component of velocity</i>)	-5 m/s	For all Configurations
		-10 m/s	
		-20 m/s	
		-40 m/s	
	-55 m/s		



(a) Coarse (b) Fine (c) Superfine
Fig 3 : Zoomed in view of Coarse, Fine and Superfine Mesh.

Summary of aerodynamics coefficients for lift, drag and pitching moment for the grids is presented in Table III. As it is clear from the summary that change in aerodynamic coefficients between fine and super fine grids is very less (0.63%, 0.61% and 0.37% for C_l , C_d and C_m respectively), therefore fine grid has been finally selected for further analyses.

TABLE III
Summary of Aerodynamic Coefficients for Grids

Grid Name	Total No of Cells	C_l	C_d	C_m	Remarks
Coarse	3.42 M	0.496	0.0302	1.669	
Fine	4.83 M	0.478	0.0324	1.609	Selected
Super Fine	5.98 M	0.475	0.0326	1.603	

V. RESULTS AND DISCUSSIONS

Effects of suction parameters on junction flow have been analyzed using the streamlines of the flow obtained on the

symmetric plane ahead of the wing leading edge. The formation of horseshoe vortex in the junction flow originates from the symmetric plane. Therefore, as already established by S Ahmed et al. [8] streamlines in this plane are meaningful parameters in the junction flow studies. Formation of vortex core can be seen near the wing leading edge and floor on observation of the streamlines and velocity vectors on the symmetry plane. This vortex is in fact a 2D representation of the horseshoe vortex which causes aerodynamic losses in the junction region.

Before proceeding to discuss the results in detail, it is important to note that obtained results for the first configuration of suction hole with a dimension of $100 \times 82 \text{ mm}^2$ located at 92 mm away from the wing leading edge was validated by comparing the numerical results with the experimental results performed by Barberis et al. [4]. Details on the validation can be found in our previous study mentioned in S. Ahmed et al. [8].

Flow patterns formed by the streamlines on the symmetry plane for the no suction case and suction with 5 m/s for the first configuration with 25 m/s incoming velocity can be seen in Fig 4 and Fig 5.

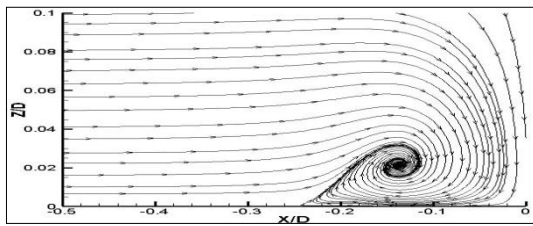


Fig 4 : Streamlines on plane of symmetry for no suction case, First configuration with 25 m/s incoming vel

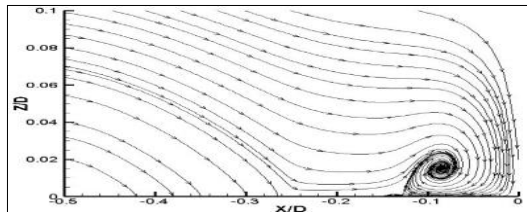


Fig 5 : Streamlines on plane of symmetry for suction rate of 5 m/s, first configuration with 25 m/s incoming velocity

Vortex core formation can be clearly seen in both Fig 4 and Fig 5. Similar flow patterns were obtained for all the cases using the streamlines and velocity vectors on the symmetry plane. Locations of vortex core formed were then compared with each other to see the effects of the suction parameters on horseshoe formation. It is important to note that the bigger size vortex and located away from the wing leading edge and floor represents the formation of stronger horseshoe vortex, whereas smaller size vortex near the wing leading edge and floor represents the formation of weaker horseshoe vortex.

Effect of suction parameters i.e., hole location and dimension and effect of incoming velocity on formation of horseshoe vortex would be discussed separately by comparing the vortex formation on the symmetry plane.

TABLE IV
Comparison of Vortex Core for First and Second Configurations of Suction Hole

Suction Rate (m/s)	Vertical Distance of Vortex Core (mm from floor)		Horizontal Distance of Vortex Core (mm from LE)	
	Suction Hole Location		Suction Hole Location	
	92 mm from LE	50 mm from LE	92 mm from LE	50 mm from LE
5	7.56	5.04	50.4	40.68
10	5.45	2.82	32.7	21.38
20	3.8	Vortex Not Formed	20.2	Vortex Not Formed
40	3.3		18.0	
55	3.2		16.1	

A. Effects of Suction Hole Location

In order to see the effect of suction hole location on formation of horseshoe vortex, results obtained by application of suction through the two sizes of suction hole placed at different positions have been compared with each other. In this regard, the first configuration with second configuration and third configuration with fourth configuration have been compared. Comparison of location of vortex core of first and second configuration in terms of distances from obstacle leading edge and floor for all suction velocities are summarized in TABLE IV; whereas, for third and fourth configuration are summarized in TABLE V. For clearer understanding graphical comparisons are shown in Fig 6, Fig 7, Fig 8 and Fig 9.

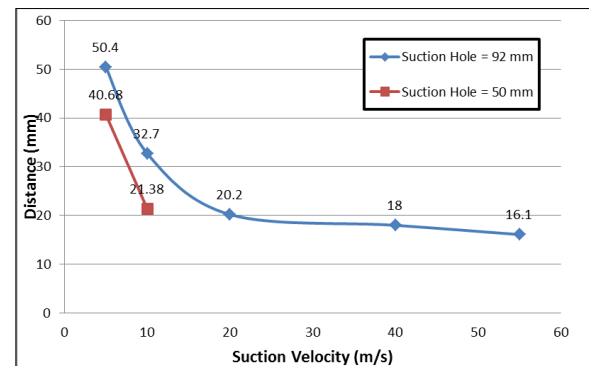


Fig 6: Comparison of Distance of Vortex Core from Model LE for 1st and 2nd Configurations

It can be seen from the table that when the suction hole was moved closer to the obstacle leading edge, smaller and weaker vortex core are formed for the given suction rates. When suction rate was increased beyond 20 m/s for the suction hole with bigger dimensions and 40 m/s for the suction hole with smaller dimensions, vortex core has disappeared depicting complete elimination of the horseshoe vortex. Graphical representation is also clearly showing the reduction in vortex core for suction rates of 5 and 10 m/s and elimination of vortex core for suction rates of 20 m/s and beyond.

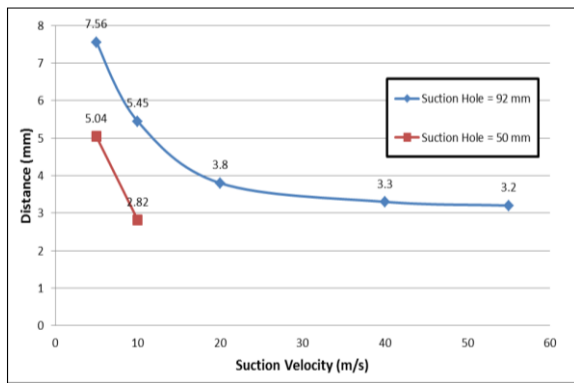


Fig 7 : Comparison of Distance of Vortex Core from Floor for 1st and 2nd Configurations

TABLE V
Comparison of Vortex Core for Third and Fourth Configurations of Suction Hole

Suction Rate (m/s)	Vertical Distance of Vortex Core (mm from floor)		Horizontal Distance of Vortex Core (mm from LE)	
	Suction Hole Location		Suction Hole Location	
	92 mm from LE	50 mm from LE	92 mm from LE	50 mm from LE
5	7.99	4.43	64.44	34.2
10	7.70	1.872	47.68	16.2
20	5.47	0.47	36.86	8.64
40	4.5	Vortex Not Formed	26.67	Vortex Not Formed
55	4.1		23.68	

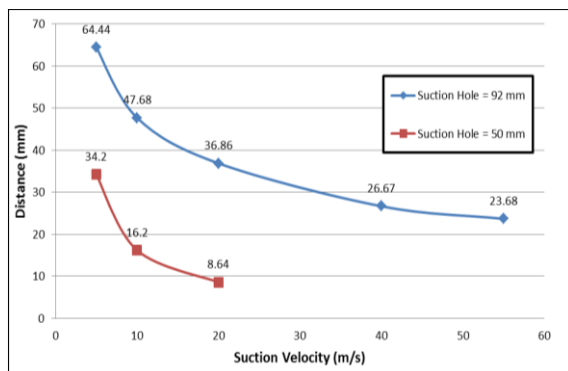


Fig 8 : Comparison of Distance of Vortex Core from Model LE for 3rd and 4th Configurations

It can therefore be concluded that suction hole when located closer to the leading edge is proved to be more effective in elimination of the vortex formation. When suction hole is located closer to the leading edge then lower suction rates are required for control of horseshoe vortex.

B. Effects of Suction Hole Dimensions

Two different dimensions of suction hole were analyzed to see the effect of suction hole size on formation of horseshoe vortex. In this regard, a hole of dimension $100 \times 82 \text{ mm}^2$ and

$50 \times 40 \text{ mm}^2$ were positioned at two different locations and compared with each other for both the locations. Location of vortex core comparison for the different suction hole dimensions when positioned at 92 mm away from the wing leading edge are given in TABLE VI. Similarly, the comparison for the different suction hole dimensions when the holes are positioned at 50 mm away from the wing leading edge are given in Table VII. Graphical comparison between horizontal and vertical distance of the vortex core location from wing leading edge and floor are shown in Fig 10 and Fig 11.

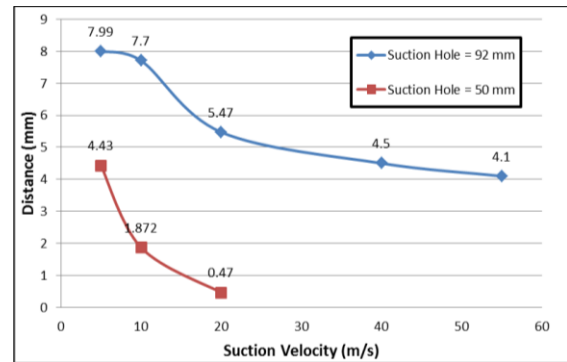


Fig 9 : Comparison of Distance of Vortex Core from Floor for 3rd and 4th Configurations

TABLE VI
Comparison of Vortex Core for Different Hole Size Located at 92 mm From Leading Edge

Suction Rate (m/s)	Vertical Distance of Vortex Core (mm from floor)		Horizontal Distance of Vortex Core (mm from LE)	
	Suction Hole Size mm ²		Suction Hole Size mm ²	
	100 × 82	50 × 40	100 × 82	50 × 40
5	7.56	7.99	50.4	64.44
10	5.45	7.70	32.7	47.68
20	3.8	5.47	20.2	36.86
40	3.3	4.5	18.0	26.67
55	3.2	4.1	16.1	23.68

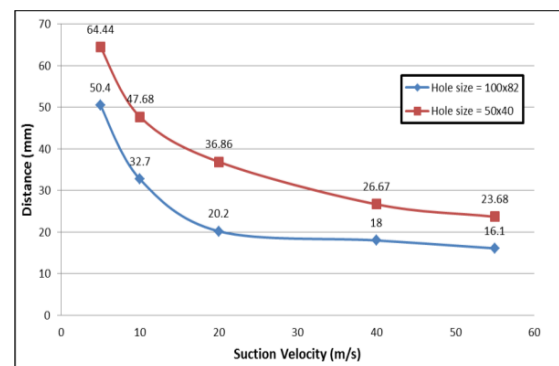


Fig 10 : Comparison of Distance of Vortex Core from Model LE for different hole dimensions located at 92 mm

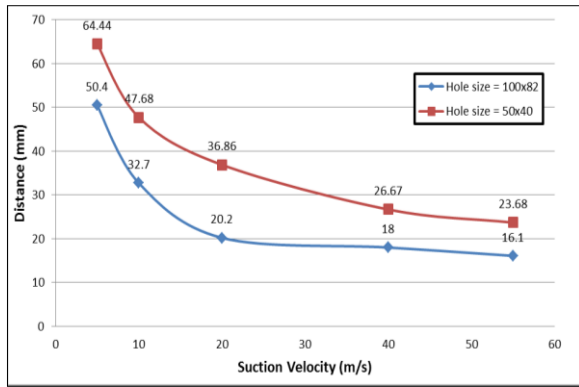


Fig 11 : Comparison of Distance of Vortex Core from Floor for different hole dimensions located at 92 mm

Analyzing the table and graphs it is clearly visible that when the suction hole dimension was reduced, the formation of vortex core was larger and away from the leading edge and floor depicting the formation of stronger horseshoe vortex for the given suction rates. When suction hole was placed at 50 mm away from the wing leading edge, vortex was eliminated for suction velocities of 20 m/s and beyond; however, with the smaller dimension of suction hole, vortex core reappeared for the suction rate of 20 m/s and was only eliminated after application of suction rates of 40 m/s and beyond. This phenomenon shows that dimension of suction hole is inversely proportional to vortex core formation for given suction rate where increasing the suction hole dimension reduces the size of the vortex core.

TABLE VII

Comparison of Vortex Core for Different Hole Size Located at 50 mm From Leading Edge

Suction Rate (m/s)	Vertical Distance of Vortex Core (mm from floor)		Horizontal Distance of Vortex Core (mm from LE)	
	Suction Hole Size mm ²		Suction Hole Size mm ²	
	100 × 82	50 × 40	100 × 82	50 × 40
5	5.04	4.43	40.68	34.2
10	2.82	1.872	21.38	16.2
20		0.47		8.64
40	Vortex Not Formed	Vortex Not Formed	Vortex Not Formed	Vortex Not Formed
55	Vortex Not Formed	Vortex Not Formed	Vortex Not Formed	Vortex Not Formed

From analyses of the data from the tables and graphs, it can be concluded that bigger dimension of suction hole proved to be more effective in controlling the horseshoe vortex as compared with the smaller dimension of suction hole. For bigger suction hole lower suction rates would produce better results compared to the suction hole with smaller dimensions.

C. Effects of Incoming Velocity

To study the effect of incoming velocity on formation of horseshoe vortex and its subsequent effect on suction, two different incoming velocities i.e., 50 m/s and 25 m/s were used for numerical simulation of the flow with and without localized suction. Remaining parameters were kept constant, and the results were compared with each other. Comparisons of location of vortex core for the two incoming velocities with different suction rates when suction hole was positioned at 92 mm away from the leading edge are given in TABLE VIII. Graphical comparison between horizontal and vertical distance of the vortex core location from wing leading edge and floor are shown in Fig 12 and Fig 14. Similarly, comparison of saddle point location is shown in Fig 14.

TABLE VIII

Comparison of Vortex Core for Different Incoming Vel for Hole Located at 92 mm From Leading Edge

Suction Rate (m/s)	Vertical Distance of Vortex Core (mm from floor)		Horizontal Distance of Vortex Core (mm from LE)		Location of Saddle Point (mm from LE)	
	Incoming Velocity		Incoming Velocity		Incoming Velocity	
	50 m/s	25 m/s	50 m/s	25 m/s	50 m/s	25 m/s
No Suction	9.2	6.87	90	48.96	138	82.35
5	7.56	5.4	50.4	30.82	78	50.91
10	5.45	3.78	32.7	20.7	46.5	37.5
20	3.8	1.35	20.2	16.34	40	21.04
40	3.3	0.54	18.0	14.65	28.4	19.54
55	3.2	Not Formed	16.1	Not Formed	25	Not Formed

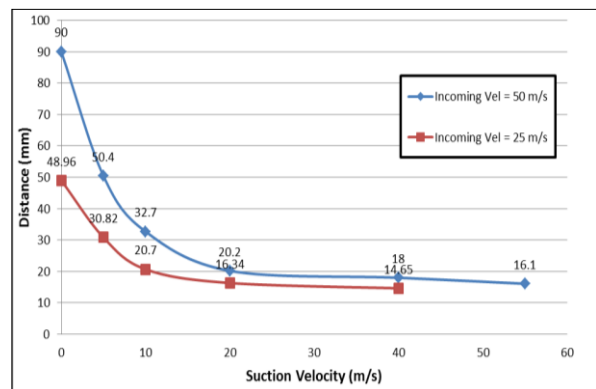


Fig 12 : Comparison of Distance of Vortex Core from Model LE for incoming vel of 50 m/s and 25 m/s

It is clear from the data presented in the table and figures that by reducing the incoming velocity the vortex size and dimensions have reduced indicating reduction in the strength of the horseshoe formation. Moreover, similar pattern of

reduction in the size of vortex have been observed with both incoming velocities when suction was applied.

By increasing suction rate, reduction in vortex size was more prominent. It can be deduced from the data that for lower incoming velocities, lower suction rates may also perform better as compared to the cases of higher incoming velocities.

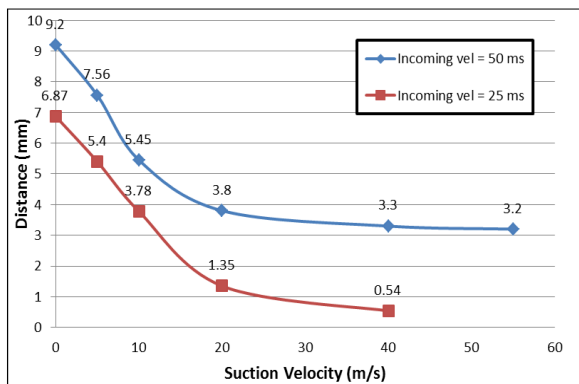


Fig 13 : . Comparison of Distance of Vortex Core from Floor for incoming vel of 50 m/s and 25 m/s

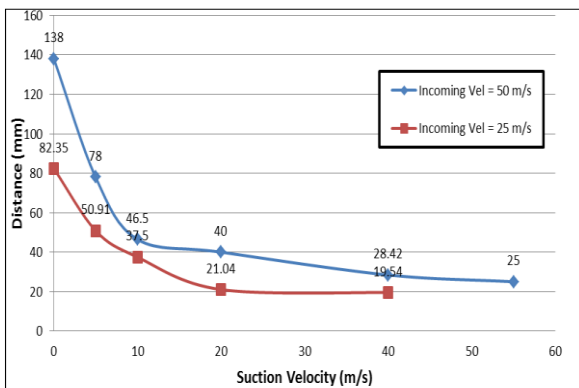


Fig 14 : Comparison of Distance of Saddle Point from Model LE for incoming vel of 50 m/s and 25 m/s

VI. CONCLUSION

During this study, effects of suction parameters in terms of suction hole location from obstacle leading edge and its dimensions on horseshoe vortex formation in junction flows were investigated. It is concluded based on the obtained results that location of suction hole has a strong influence on formation of horseshoe vortex. Positioning the suction hole closer to the wing leading edge proves to be more effective in elimination of horseshoe vortex as lower suction rates are required to eliminate the vortex core in comparison to when suction hole is positioned away from the leading edge. Similarly, suction hole dimensions also influence the formation of horseshoe vortex. Bigger dimension of suction hole proved to be more effective in controlling the horseshoe vortex as compared with the smaller dimension of suction hole. Finally, it was found that vortex formation is stronger for higher incoming velocities and therefore, for lower incoming velocities lower suction rates are sufficient to get the same effect of horseshoe vortex control as compared to the higher incoming velocities.

Study can be extended to see the effect of wing sweep and angle of attack on formation of horseshoe vortex. Moreover, shape of suction hole may also be evaluated for optimization of suction configuration. Results obtained can then be utilized along with the results obtained during this study to recommend an optimized geometry and location of suction hole for application in junction flows which may work for all wing sweeps, angle of attacks and incoming velocities.

ACKNOWLEDGMENT

The authors would like to acknowledge Department of Aeronautics and Astronautics, Institute of Space Technology, Islamabad for providing administrative and technical support for undertaking this research work.

REFERENCES

- [1] F. Gand, S. Deck, V. Brunet, and P. Sagaut, "Flow dynamics past a simplified wing body junction," *Physics of Fluids*, vol. 22, p. 115111, 2010.
- [2] J. L. Fleming, R. Simpson, J. Cowling, and W. Devenport, "An experimental study of a turbulent wing-body junction and wake flow," *Experiments in fluids*, vol. 14, pp. 366-378, 1993.
- [3] D. Philips, J. Cimbala, and A. Treaster, "Suppression of the wing-body junction vortex by body surface suction," *Journal of aircraft*, vol. 29, pp. 118-122, 1992.
- [4] D. Barberis, P. Molton, and T. Malaterre, "Control of 3D turbulent boundary layer separation caused by a wing-body junction," *Experimental thermal and fluid science*, vol. 16, pp. 54-63, 1998.
- [5] R. Paciorri, A. Bonfiglioli, A. Di Mascio, and B. Favini, "RANS simulations of a junction flow," *International Journal of Computational Fluid Dynamics*, vol. 19, pp. 179-189, 2005.
- [6] J. L. Coombs, C. J. Doolan, D. J. Moreau, A. Zander, and L. Brooks, "Assessment of turbulence models for a wing-in-junction flow," *Assessment*, vol. 3, p. 7, 2012.
- [7] A. Levchenya, E. Smirnov, and V. Goryachev, "RANS-based numerical simulation and visualization of the horseshoe vortex system in the leading edge endwall region of a symmetric body," *International Journal of Heat and Fluid Flow*, vol. 31, pp. 1107-1112, 2010.
- [8] S. Ahmed, A. Malik, and K. Parvez, "RANS Predictions of Junction Flow with Localized Suction," in *2018 IEEE International Conference on Aerospace Electronics and Remote Sensing Technology (ICARES)*, 2018, pp. 1-7.
- [9] P. Spalart and S. Allmaras, "A one-equation turbulence model for aerodynamic flows," in *30th aerospace sciences meeting and exhibit*, 1992, p. 439.
- [10] C. Fluent-Commercial, "software package based on finite Volume Method," *Fluent Inc., Centerra Resource Park*, vol. 10.
- [11] J. B. Lee, D. H. Shin, J. H. Moon, and S. H. LEE, "FLUENT 6.3. 26 User's Guide FLUENT 6.3. 26 User's Guide," *Materials transactions*, vol. 53, pp. 2043-2048, 2012.